Supporting Information

Metallic PtC monolayer as a promising hydrogen evolution electrocatalyst

Huan Lou[1*], and Chi Ma[2]

[1]*Department of Applied Physics, School of Science, Jiangsu University of Science and Technology, Zhenjiang 212100, China*

[2]*Department of Optoelectronic Information of Science and Engineering, School of Science, Jiangsu University of Science and Technology, Zhenjiang 212100, China*

Corresponding Author
*E-mail: louhuan@just.edu.cn

Index	Page

Computational Details

The particle swarm optimization (PSO) method within the evolutionary algorithm implemented in the Crystal structure AnaLYsis by Particle Swarm Optimization (CALYPSO) code[1,2] was employed to find the lowest energy structures of the PtC_x (x = 1-4) monolayers. Unit cells containing 1, 2, and 4 formula units (f.u.) were considered. In the first step, random structures with certain symmetry are constructed in which atomic coordinates are generated by the crystallographic symmetry operations. Local optimizations using the VASP code[3] were done with the conjugate gradients method and stopped when Gibbs free energy changes became smaller than 1×10^{-5} eV per cell. After processing the first-generation structures, 60% of them with lower Gibbs free energies are selected to construct the next generation structures by Particle Swarm Optimization (PSO). 40% of the structures in the new generation are randomly generated. A structure fingerprinting technique of bond characterization matrix is applied to the generated structures, so that identical structures are strictly forbidden. These procedures significantly enhance the diversity of the structures, which is crucial for structural global search efficiency. In most cases, structural searching simulations for each calculation were stopped after generating 1000 ~ 1200 structures (*e.g.* about 20-30 generations).

The local structural relaxations and electronic properties calculations were performed in the framework of the density functional theory (DFT)[4] within the generalized gradient approximation (GGA)[5] as implemented in the VASP code. The cut off energy is 500 eV for plane-wave expansions, the total energy and force convergence precision are set to 10^{-5} eV and 10^{-2} eV/Å. Moreover, Van der Waals interactions (DFT-D2) is employed.[6] The valence orbitals of Pt and C atoms are $6s^1 5d^9$ and $2s^2 2p^2$, respectively.

First-principles molecular dynamics (MD)[7] simulations for a large supercell were performed at different temperatures of 300 K. The supercells adopt $1 \times 3 \times 3$ for PtC with $P2_1/m$ symmetry, $3 \times 1 \times 1$ for PtC_2 with *Pbam* symmetry, $5 \times 1 \times 1$ for PtC_3 with *Pma*2 symmetry, and $1 \times 3 \times 1$ for PtC_4 with *Pbam* symmetry. MD simulation in NVT ensemble lasted for 10 ps with a time step of 1.0 fs. The temperature was controlled by using the Nosé-Hoover method.

The HER performance of the PtC_x (x = 1-4) monolayers are studied by the differential Gibbs free energy of hydrogen adsorption,[8] *i.e.* $\Delta G_{H*} = \Delta E_H + \Delta E_{ZPE} - T\Delta S_H$. The adsorption energy types of H

are divided into chemisorption and average energies, of which are defined as d-$\Delta E_H = E_{PtCx+nH}$ − $E_{PtCx+(n-1)H}$ − $\frac{1}{2}E_{H2}$, and a-$\Delta E_H = (E_{PtCx+nH} - E_{PtCx} - \frac{1}{2}nE_{H2})/n$, respectively. $E(PtC_x+nH)$ and E_{H2} are the total energies of PtC_x adsorbing n H and a H_2, respectively. ΔE_{ZPE} and ΔS_H are zero-point energy difference and entropy difference between adsorbed H and H_2, T is room temperature, among ΔE_{ZPE} − $T\Delta S_H$ is given 0.24 eV.[8] Therefore, there are two HER processes, *i.e.* individual process describes the production of H_2 molecule one by one (d-ΔG_{H*}), and average process shows all H atoms are simultaneously converted to H_2 (a-ΔG_{H*}) on the basal surface. The theoretical exchange current (i_0) is calculated as[9]

$$i_0 = \begin{cases} \dfrac{-ek_0}{1 + exp\left[-\dfrac{\Delta G_{H*}}{k_bT}\right]}, & \Delta G_{H*} \leq 0 \\[3em] \dfrac{-ek_0}{1 + exp\left[\dfrac{\Delta G_{H*}}{k_bT}\right]}, & \Delta G_{H*} \geq 0 \end{cases}$$

where the rate constant k_0 is presumed 1.

Cohesive energy

Cohesive energy is widely used to ascertain the feasibility for experimental synthesis of the predicted 2D materials. Here, the cohesive energy E_{coh} is calculated based on the equation of $E_{coh} = (E_{Pt} + x \times E_C - E_{PtC_x})/(1 + x)$, where E_{Pt} and E_C for Pt and C atoms are the enthalpy values of each single atom placed in a $10 \times 10 \times 10$ Å box. E_{PtC_x} is the energy of 2D PtC_x unit cell.

Dissolution potential U_{diss}

The electrochemical stability of the PtC_x monolayers is assessed by the dissolution potential U_{diss}, which are defined as

$$E_f = (E_{PtCx} - E_{Pt} - E_C)/2$$

$$U_{diss} = U_{diss}^0(metal, bulk) - E_f/ne$$

where E_f is formation energy, E_{PtC_x} E_{Pt}, and E_C represent the energies of the PtC_x monolayer, the Pt and C atoms in bulk structure, respectively. U_{diss}^0(metal, bulk) and n stand for the standard dissolution potential of bulk metal and the number of electrons involved in the dissolution, respectively.

Effect of pH on HER performance

$\Delta G(pH) = k_B T \ln(10) \times pH$

$\Delta G(pH)$ is an additional barrier for the adsorption of H atoms and is given by the pH value of the electrolyte. $\Delta G(pH)$ value equals to 0 eV when pH = 0 and increases when the corresponding electrolyte is neutral or basic.
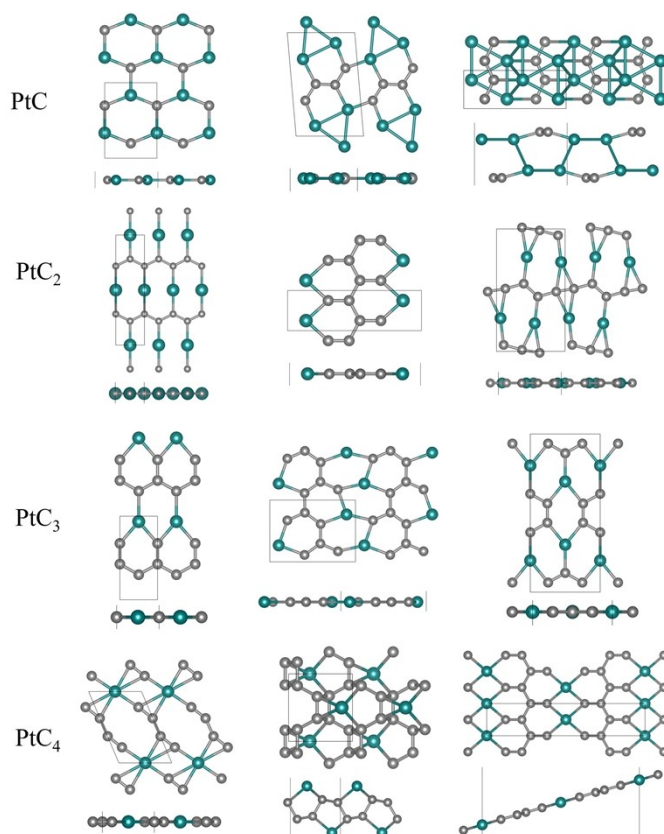
Supporting Figures

Figure S1. Top and side views of selected low-energy configurations for each monolayer ratio. The indigo and gray balls represent Pt and C atoms, respectively.
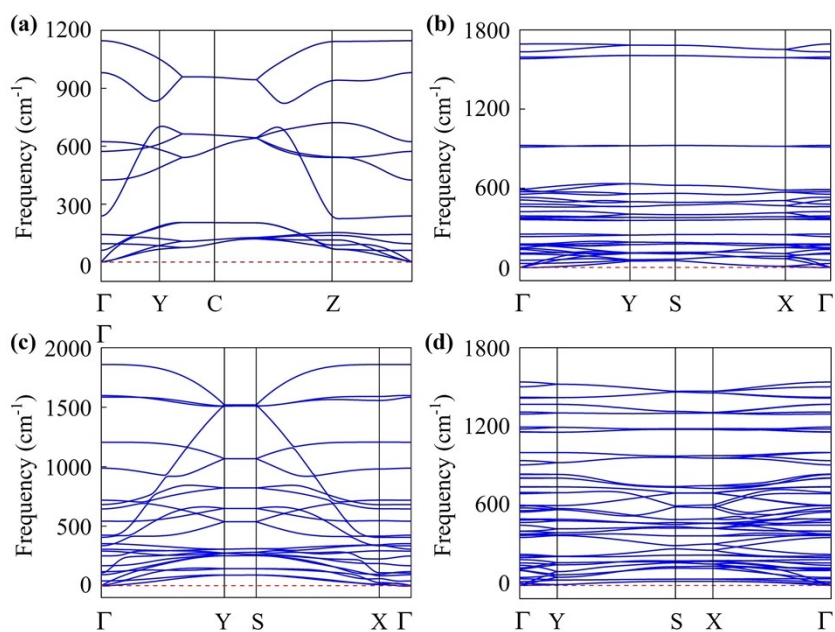

Figure S2. Phonon dispersive curves of the (a) PtC, (b) PtC_2, (c) PtC_3, and (d) PtC_4 monolayers. The phonon maximum frequencies of four monolayers are 1146, 1693, 1859, and 1540 cm^{-1}, respectively.
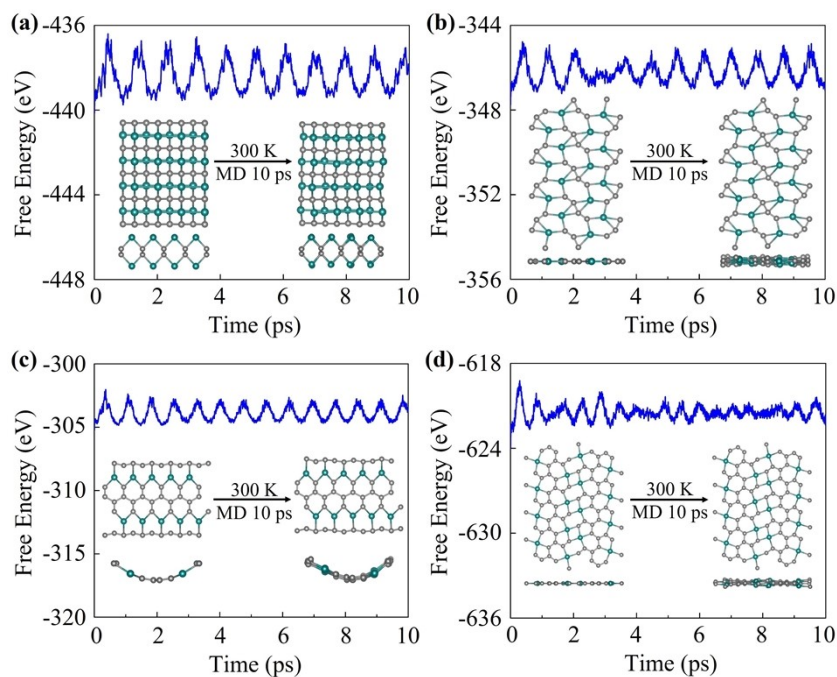
Figure S3. Snapshots of the final frame of the PtC$_x$ monolayers at time of 10 ps during AIMD simulations under the temperatures of 300 K, (a) PtC, (b) PtC$_2$, (c) PtC$_3$, and (d) PtC$_4$ monolayers. The indigo and gray balls represent Pt and C atoms, respectively.
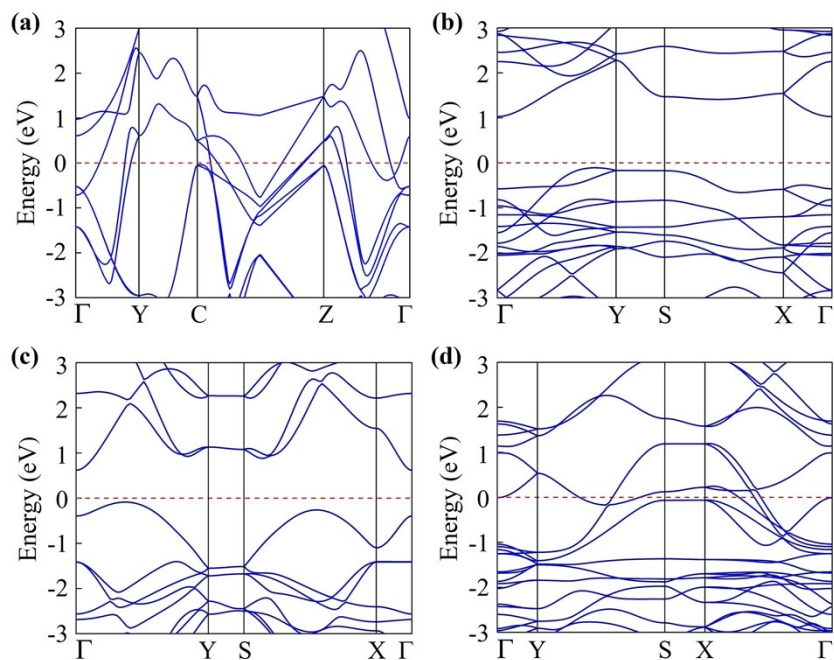

Figure S4. Band structures of the (a) PtC, (b) PtC$_2$, (c) PtC$_3$, and (d) PtC$_4$ monolayers. The red solid lines represent the Fermi level.
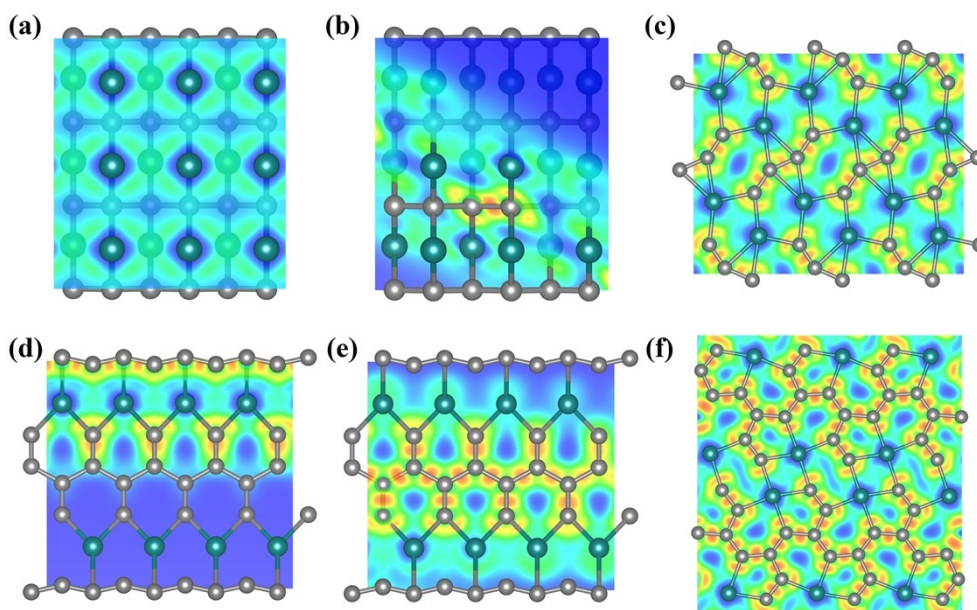
Figure S5. Electron localization function (ELF) map and crystal structures of the (a-b) PtC, (c) PtC$_2$, (d-e) PtC$_3$, and (f) PtC$_4$ monolayers. The indigo and gray balls represent Pt and C atoms, respectively.

Figure S6. Calculated differential Gibbs free energies as a function of H coverage of the PtC$_4$ monolayers for H adsorbed on T$_{C3}$ site when pH = 0 at T = 300K. (a) d-ΔG_{H*} and (b) a-ΔG_{H*}. The highlighted in green denotes the free energy window of $\pm$ 0.25 eV.

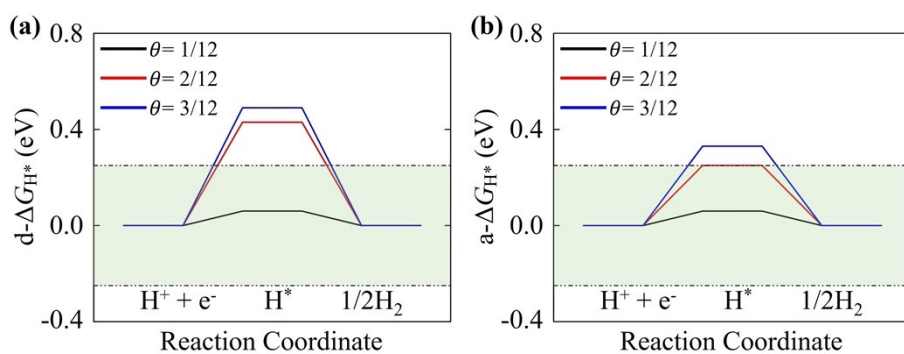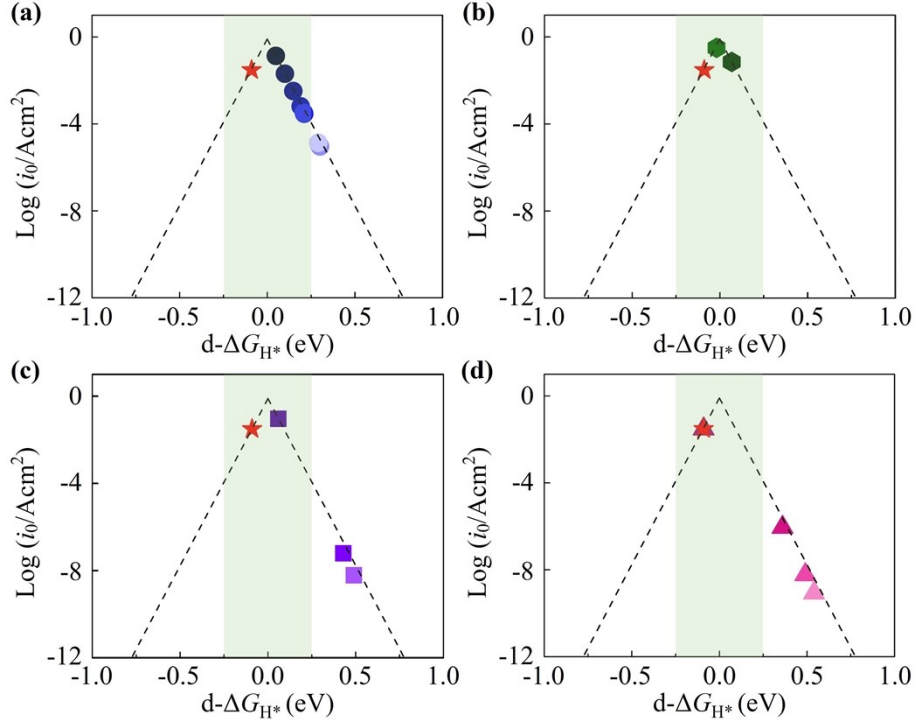**Figure S7.** Volcano curve of exchange current density i_0 of the (a) PtC, (b) PtC_2, (c) T_{C3} site, and (d) T_{Pt} site of the PtC_4 monolayers as a function of d-ΔG_{H*} when pH = 0 at T = 300K. The value of Pt is inserted by a red star for comparison. The color changes from dark to light with increasing H coverage.
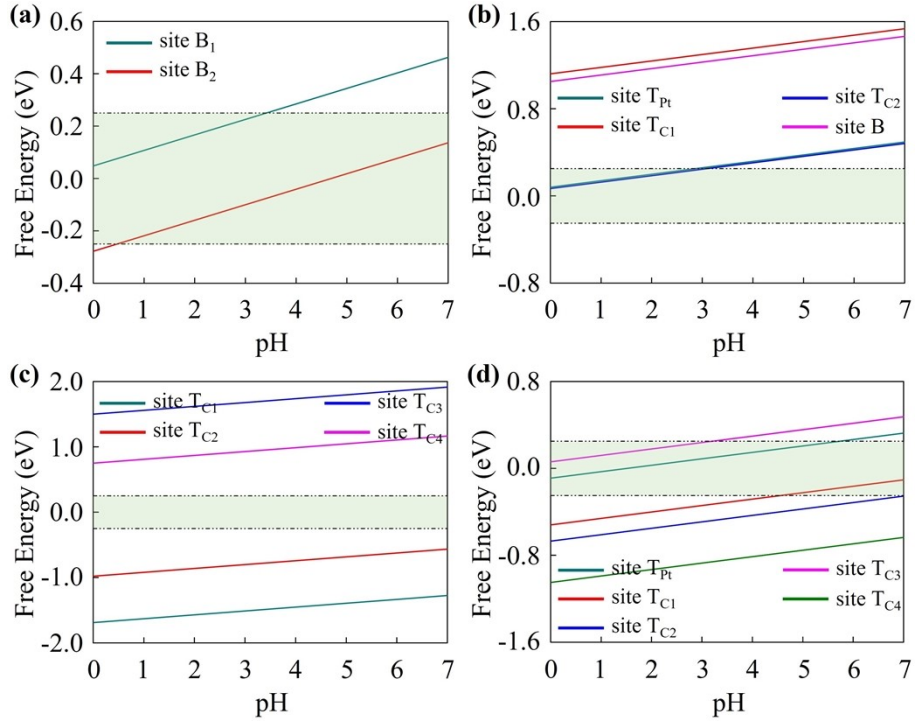
Figure S8. Free energy of Hydrogen adsorption as a function of the pH value for the (a) PtC, (b) PtC_2, (c) PtC_3, and (d) PtC_4 monolayers. A $\pm$ 0.25 eV window is indicated in green.
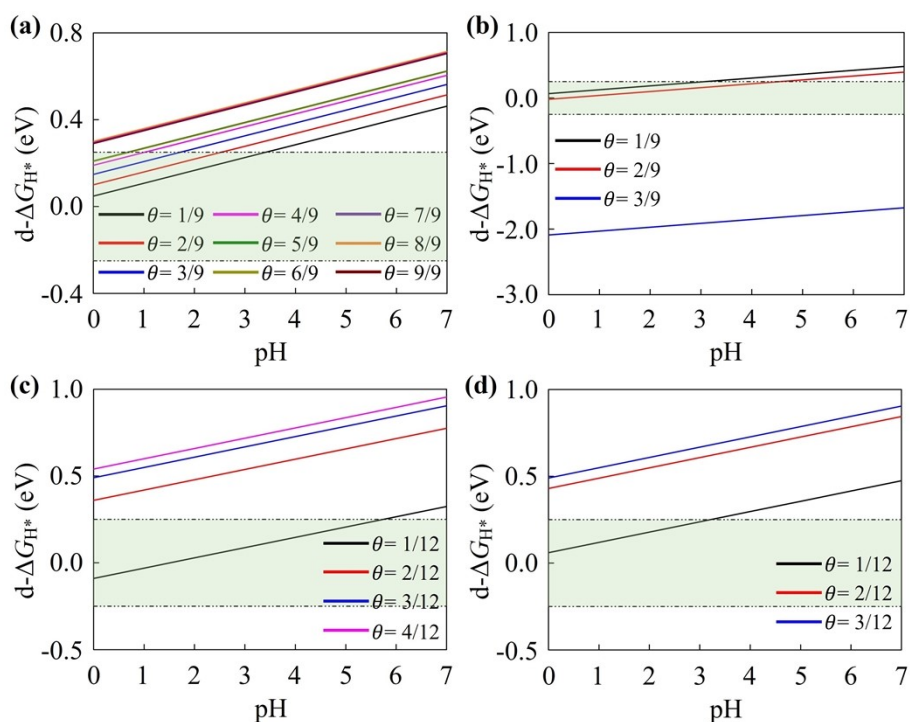
Figure S9. d-ΔG_{H*} as a function of the pH value for the (a) PtC, (b) PtC$_2$, H adsorbed on (c) T$_{Pt}$ site and (d) T$_{C3}$ of PtC$_4$ monolayers. A $\pm$ 0.25 eV window is indicated in green.

Figure S10. Exchange current density as a function of the pH value for the (a) PtC, (b) PtC$_2$, and (c) PtC$_4$ monolayers for H adsorption sites.

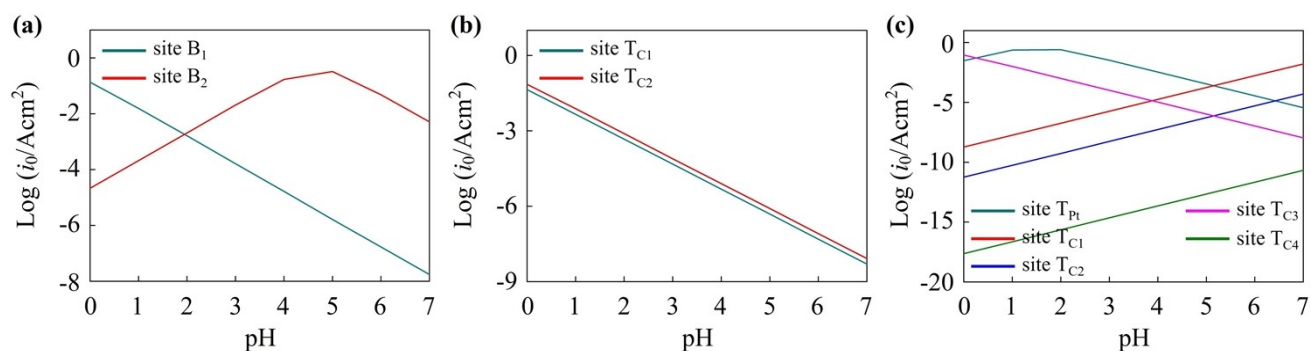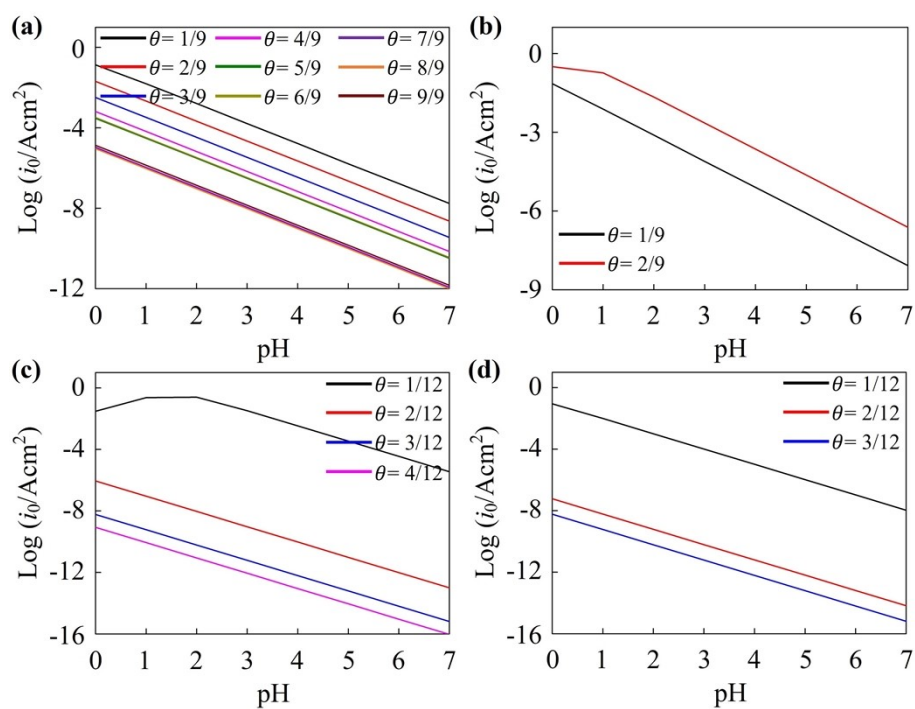**Figure S11.** Exchange current density as a function of the pH value with various H coverage for the (a) PtC, (b) PtC$_2$, H adsorbed on (c) T$_{Pt}$ site and (d) T$_{C3}$ of PtC$_4$ monolayers based on d-ΔG_{H*}.

Supporting Tables

Table S1. Structural information of the predicted PtC$_x$ (x = 1-4) monolayers.

Phase	Space Group	Lattice Parameters (Å, °)	Wyckoff Positions	Fractional Coordinates		
				x	y	z
PtC	$P2_1/m$	a = 22.25840	Pt(2e)	0.58453	0.75000	0.47651
		b = 2.58700	C(2e)	0.51699	0.75000	0.99528
		c = 2.79880				
		α = 90.0000				
		β = 87.9914				
		γ = 90.0000				
PtC$_2$	$Pbam$	a = 4.29970	Pt(4h)	0.27718	0.82813	0.50000
		b = 10.52200	C$_1$(4h)	0.82317	0.86806	0.50000
		c = 30.00000	C$_2$(4h)	0.84773	0.47230	0.50000
		α = 90.0000				
		β = 90.0000				
		γ = 90.0000				
PtC$_3$	$Pma2$	a = 2.61830	Pt(2c)	0.25000	0.81524	0.50426
		b = 9.69370	C$_1$(2c)	0.25000	0.46281	0.46835
		c = 21.18650	C$_2$(2c)	0.75000	0.67505	0.47780
		α = 90.0000	C$_3$(2c)	0.75000	0.98508	0.56060
		β = 90.0000				
		γ = 90.0000				
PtC$_4$	$Pbam$	a = 14.73520	Pt(4h)	0.57598	0.85443	0.50000
		b = 4.65800	C$_1$(4h)	0.29214	0.99290	0.50000
		c = 29.75800	C$_2$(4h)	0.37368	0.54335	0.50000
		α = 90.0000	C$_3$(4h)	0.28489	0.67294	0.50000
		β = 90.0000	C$_4$(4h)	0.44532	0.71920	0.50000
		γ = 90.0000				

Table S2. Cohesive energy (E_{coh}) of the predicted PtC$_x$ (x = 1-4) monolayers.

Pt-C monolayer	E_{coh} (eV)
PtC	6.62
PtC$_2$	6.41
PtC$_3$	6.75
PtC$_4$	6.79

Table S3. Mulliken charge (|e|) analysis of the PtC$_x$ (x = 1-4) monolayers.

Atom	PtC Charge (|e|)	PtC ΔG_{H*} (eV)	PtC$_2$ Charge (|e|)	PtC$_2$ ΔG_{H*} (eV)	PtC$_3$ Charge (|e|)	PtC$_3$ ΔG_{H*} (eV)	PtC$_4$ Charge (|e|)	PtC$_4$ ΔG_{H*} (eV)
Pt	0.42	B$_1$(Pt-Pt) 0.05	1.03	1.05	0.96	-	1.17	-0.09
C$_1$	-0.42	B$_2$(Pt-Pt) -0.28	-0.67	0.08	-0.52	0.75	-0.32	-0.52
C$_2$			-0.36	0.06	-0.10	1.50	-0.34	-0.67
C$_3$			B(Pt-Pt) 1.12		-0.68	-0.98 -1.69	-0.01	0.06
C$_4$							-0.50	-1.05

Table S4. Calculated d-ΔG_{H*} and a-ΔG_{H*} (eV) varying different H atoms (n) adsorbed on the PtC$_x$ (x = 1-4) monolayers.

n site	PtC B$_1$		PtC$_2$ T$_{C2}$		PtC$_3$ T$_{C1}$		PtC$_4$ T$_{C3}$		PtC$_4$ T$_{Pt}$	
1	0.05	0.05	0.06	0.06	0.75	0.75	0.06	0.06	-0.09	-0.09
2	0.10	0.07	-0.02	-0.02			0.43	0.25	0.36	0.13
3	0.15	0.10	-2.09	-0.07			0.49	0.33	0.49	0.25
4	0.19	0.12							0.54	0.33
5	0.21	0.14								
6	0.21	0.15								
7	0.29	0.17								
8	0.30	0.19								
9	0.29	0.20								

References

1   Y. Wang, J. Lv, L. Zhu and Y. Ma, CALYPSO: A method for Crystal Structure Prediction, *Comput. Phys. Commun.*, 2012, **183**, 2063–2070.

2   Y. Wang, J. Lv, L. Zhu and Y. Ma, Crystal Structure Prediction Via Particle-Swarm Optimization, *Phys. Rev. B.*, 2010, **82**, 094116.

3   G. Kresse and J. Furthmüller, Efficient Iterative Schemes for Ab Initio Total-Energy Calculations Using A Plane-Wave Basis Set, *Phys. Rev. B*, 1996, **54**, 11169–11186.

4   J. Y. Jung, J. H. Park, Y. J. Jeong, K. H. Yang, N. K. Choi, S. H. Kim and W. J. Kim, Self-Consistent Equations Including Exchange and Correlation Effects, *Phys. Rev.*, 1965, **140**, A1133–A1138.

5   J. P. Perdew, K. Burke and M. Ernzerhof, Generalized Gradient Approximation Made Simple, *Phys. Rev. Lett.*, 1996, **77**, 3865–3868.

6   S. Grimme, Accurate Description of Van Der Waals Complexes by Density Functional Theory Including Empirical Corrections, *J. Comput. Chem.*, 2004, **25**, 1463–1473.

7   G. J. Martyna, M. L. Klein and M. Tuckerman, Nosé-Hoover Chains: The Canonical Ensemble Via Continuous Dynamics, *J. Chem. Phys.*, 1992, **97**, 2635–2643.

8   Y. Shao, X. Shi and H. Pan, Electronic, Magnetic, and Catalytic Properties of Thermodynamically Stable Two-Dimensional Transition-Metal Phosphides, *Chem. Mater.*, 2017, **29**, 8892–8900.

9   B. Zhang, X. Fu, L. Song and X. Wu, Improving Hydrogen Evolution Reaction Performance by Combining Ditungsten Carbide and Nitrogen-Doped Graphene: A First-Principles Study, *Carbon N. Y.*, 2021, **172**, 122–131.